ACS APPLIED MATERIALS & INTERFACES

Letter

www.acsami.org

Synthesis of Zn:Cu_2O Thin Films Using a Single Step Electrodeposition for Photovoltaic Applications

Changqiong Zhu and Matthew J. Panzer*

Department of Chemical & Biological Engineering, Tufts University, 4 Colby Street, Medford, Massachusetts 02155, United States

Supporting Information

ABSTRACT: Zinc-doped cuprous oxide (Zn:Cu_2O) thin films have been prepared via single step electrodeposition from an aqueous solution containing sodium perchlorate. The Zn/Cu molar ratio in the Zn:Cu_2O films can be tuned between 0.006 and 0.236 by adjusting the magnitude of the applied potential and the sodium perchlorate concentration. Electrical characterization reveals that zinc dopants increase the Fermi level in Zn:Cu_2O films, enabling a 3-fold improvement in the power conversion efficiency of a fully electrodeposited Cu_2O homojunction photovoltaic device.

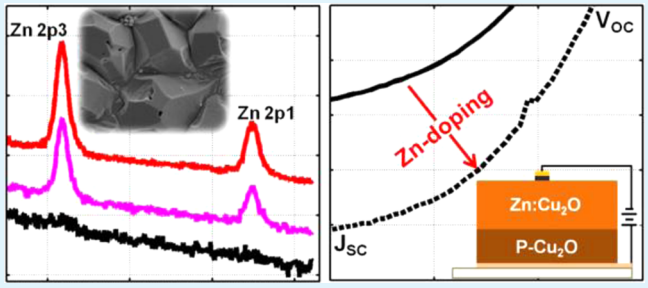

KEYWORDS: *metal oxides, cation dopants, ZnO, coelectrodeposition, sodium perchlorate*

Cuprous oxide (Cu_2O) is a nontoxic, earth abundant, p-type semiconductor with a direct band gap of ~2.0 eV and an absorption coefficient exceeding 10^5 cm^{-1} at 450 nm, which has prompted its investigation as a promising material for photocatalysis and photovoltaics (PVs).[1−10] Several groups have recently explored the use of electrodeposition as a low energy, scalable, and attractive solution-based method of forming Cu_2O thin films for PV devices.[6−10] Importantly, the electrodeposition conditions used (pH, ligand chemistry) are now understood to substantially alter the morphology, preferred crystalline orientation, and optoelectronic properties of the Cu_2O films. Clear p-type character (Fermi level ~0.2−0.4 eV above the valence band maximum, which is located 5.2 eV below vacuum)[9] is obtained for Cu_2O films that are electrodeposited from basic solutions (pH >10) containing lactate as a chelating agent. In contrast, Cu_2O films electrodeposited from acidic solutions (pH ~5−6) containing acetate anions result in films that exhibit reduced p-type character (due to partial compensation), with the Fermi level shifted closer to the middle of the band gap, ~4.3−4.5 eV below vacuum.[9] Simple control over the Fermi level position by tuning the electrodeposition bath pH has naturally led some researchers to fabricate what have been described as p-Cu_2O/n-Cu_2O homojunctions, which exhibit a diode-like current−voltage characteristic and a clear PV response.[6−10] In 2009, Han and co-workers reported an electrodeposited Cu_2O homojunction PV device that showed a power conversion efficiency (PCE) of 0.1%;[7] soon afterward, McShane et al. reported an efficiency of 0.29% by controlling the surface morphology of the p-Cu_2O layer[6] and then obtained a device with a PCE of 1.06% through further refinement and optimization.[9]

Cation doping of metal oxides such as Cu_2O is an important mechanism by which one can tune their optoelectronic properties to enhance performance.[11−16] Theoretical work has suggested that Zn and Ni can form n- and p-type dopants in Cu_2O,[14] respectively, which may prove valuable for preparing p-n Cu_2O homojunction photovoltaic devices. The potential of Zn as a dopant to improve Cu_2O photoconductivity has also been predicted using density functional theory by Isseroff and Carter.[15] Despite the promising benefits, achieving cation doping in electrodeposited Cu_2O thin films, which feature low-energy, scalable, aqueous solution-based processing, has rarely been achieved experimentally.[16] Cation doping in electrodeposited metal oxides in general is known to occur via coelectrodeposition of two different metal oxides (host and dopant).[17,18] Notably, anion doping of electrodeposited Cu_2O with chloride has been achieved by the simultaneous codeposition of Cu_2O and CuCl.[19,20]

To understand the challenge of cation doping in Cu_2O by coelectrodeposition, it should be recalled that there are two common categories of cathodic electrodeposition of metal oxides.[21] In the first category, the redox active precursor is a metal cation that is directly reduced to form an insoluble metal oxide near the surface of the working electrode. One example is Cu_2O, which can be electrodeposited through the reduction of Cu^{2+} to Cu^+ within a potential window of approximately +0.02 V to −0.4 V vs Ag/AgCl;[6,10,22,23] larger negative applied potentials result in the further reduction of Cu^+ to metallic Cu^0. In the second category, the redox active agent is an oxidant, such as O_2 or NO_3^-, which creates a local pH increase upon being reduced at the working electrode, facilitating the deposition of a metal oxide film via precipitation of the insoluble metal hydroxide. A prime example here is ZnO, which can be electrodeposited within a potential window of

Received: January 21, 2015
Accepted: March 5, 2015
Published: March 5, 2015

DOI: 10.1021/acsami.5b00643
ACS Appl. Mater. Interfaces 2015, 7, 5624−5628

approximately −0.6 V to −2 V vs Ag/AgCl[24,25] using NO_3^- as the redox agent, leaving the valence of Zn^{2+} unchanged. Comparison of these two potential ranges typically used to electrodeposit Cu_2O and ZnO, respectively, underscores the challenge in realizing their coelectrodeposition.

In this work, we demonstrate a novel method to successfully realize the codeposition of ZnO and Cu_2O using a single step electrodeposition by introducing a strong oxidant, sodium perchlorate ($NaClO_4$), into the deposition solution. Sodium perchlorate enables the codeposition of ZnO by facilitating a local pH increase at the working electrode surface within the lower energy potential window suitable for Cu_2O electrodeposition. Homojunction photovoltaic devices containing an electrodeposited p-Cu_2O bottom layer and an electrodeposited Zn:Cu_2O top layer have been observed to clearly outperform devices containing an undoped Cu_2O top layer.

Zn:Cu_2O thin films were electrodeposited from acidic aqueous solutions (pH 5.8) containing copper(II) sulfate pentahydrate, sodium acetate, zinc nitrate, and varying amounts of sodium perchlorate (see Supporting Information for full experimental details). We have found that sodium perchlorate plays a critical role in enabling the codeposition of ZnO and Cu_2O. X-ray photoelectron spectroscopy (XPS) spectra reveal no detectable amount of zinc in Cu_2O films electrodeposited from solutions containing the zinc precursor ($Zn(NO_3)_2$) in the absence of sodium perchlorate. This can be explained by considering the series of reactions shown in Scheme 1.

Scheme 1. Proposed Reactions Yielding Co-Deposition of Cu_2O and ZnO

$$ClO_4^- + 2H^+ + 2e^- \leftrightarrow ClO_3^- + H_2O \quad (1)$$

$$2ClO_3^- + 12H^+ + 10e^- \leftrightarrow Cl_{2(g)} + 6H_2O \quad (2)$$

$$Cl_{2(g)} + 2e^- \leftrightarrow 2Cl^- \quad (3)$$

$$Zn^{2+} + 2H_2O \leftrightarrow Zn(OH)_{2(s)} + 2H^+ \leftrightarrow ZnO_{(s)} + H_2O + 2H^+ \quad (4)$$

$$Cu^{2+} + e^- \leftrightarrow Cu^+ \quad (5)$$

$$2Cu^+ + 2H_2O \leftrightarrow 2CuOH_{(s)} + 2H^+ \leftrightarrow Cu_2O_{(s)} + H_2O + 2H^+ \quad (6)$$

As a strong oxidant, sodium perchlorate can be readily reduced at the surface of the working electrode, producing additional oxidant species (such as ClO_3^- and Cl_2) with lower valence states, as shown in reactions (1), (2), and (3). During the reduction processes described by reactions (1) and (2), protons at the surface of the working electrode are consumed, which leads to a local pH increase that drives reaction (4) forward, yielding the successful deposition of ZnO on the electrode surface. Simultaneously, Cu^{2+} is reduced to Cu^+ as shown in reaction (5), leading to Cu_2O deposition via reaction (6). It should be noted that the local pH increase achieved through the reduction of perchlorate also drives the reaction (6) forward; however, to increase the rate of Cu_2O deposition, reduction of Cu^{2+} is a prerequisite step (reaction (5)). Thus, through the combined actions of perchlorate and Cu^{2+} reduction, the successful codeposition of ZnO and Cu_2O can be achieved using a single step electrodeposition process.

We have observed that the amount of zinc incorporated into the Cu_2O film can be controlled by adjusting the magnitude of the applied cathodic potential and the initial concentration of sodium perchlorate added to the solution. Figure 1a displays the Zn 2p region of the XPS spectra for films electrodeposited from solutions with an initial sodium perchlorate concentration

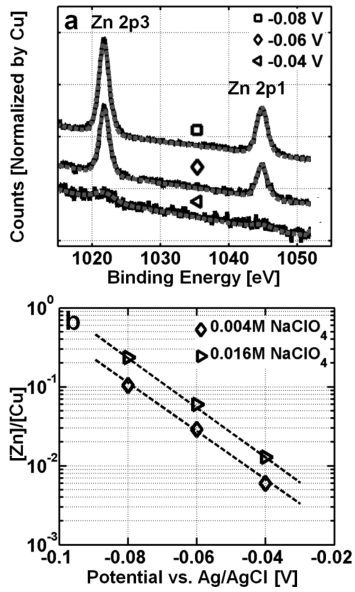

Figure 1. (a) XPS Zn 2p spectra of films electrodeposited using a $NaClO_4$ concentration of 0.004 M at applied potentials of −0.04, −0.06, and −0.08 V vs Ag/AgCl; both the raw spectra (black solid lines) and the instrument software-fitted spectra (gray dashed lines) are shown. (b) Calculated Zn/Cu molar ratio values ([Zn]/[Cu]) of Zn:Cu_2O films electrodeposited from solutions containing initial $NaClO_4$ concentrations of 0.004 and 0.016 M at applied potentials of −0.04, −0.06, and −0.08 V vs Ag/AgCl. Dashed lines represent best-fit exponential functions for each series.

of 0.004 M and applied potentials of −0.04, −0.06, and −0.08 V (vs Ag/AgCl); clear Zn 2p peak assignments demonstrate the presence of zinc. Although the Zn 2p3 peak position of pure ZnO has been reported to be located at 1022.4 eV,[26−28] Figure 1a shows that the Zn 2p3 peak positions in these Zn:Cu_2O films are centered around 1021.8 eV. We interpret this shift to indicate that incorporated zinc does not exist as regions of pure ZnO but is instead likely present as Zn^{2+} interstitials or Zn−O−Cu bridges within the Cu_2O lattice.[29] XPS Cu 2p3/2 spectra of two typical Zn:Cu_2O films and a pure Cu_2O film (obtained using 0 M $NaClO_4$) are shown in Figure S1 (Supporting Information).

Figure 1b shows the experimental Zn/Cu molar ratio values ([Zn]/[Cu]) achieved in six Zn-doped Cu_2O films as a function of applied potential for two different $NaClO_4$ concentrations. When the magnitude of the cathodic potential was increased from −0.04 to −0.08 V vs Ag/AgCl, [Zn]/[Cu] in the films electrodeposited from solutions containing 0.004 or 0.016 M $NaClO_4$ increased from 0.006 to 0.105, and from 0.013 to 0.236, respectively. For a given perchlorate concentration, [Zn]/[Cu] is seen to increase exponentially with more negative applied potential. This implies that larger cathodic potentials accelerate the relative rate of ZnO deposition (reactions (1−4)) more swiftly than that of Cu_2O deposition (reactions (5) and (6)). In addition to the applied potential, [Zn]/[Cu] is also seen to depend on the initial amount of sodium perchlorate present in the solution, although the dependence is weaker. As shown in Figure 1b, increasing the sodium perchlorate concentration by a factor of 4 (0.016 vs 0.004 M) resulted in an ∼2-fold increase in [Zn]/[Cu] for a given applied potential. It should also be emphasized that zinc is incorporated uniformly at approximately the same doping concentration throughout the entire film thickness (nominally

DOI: 10.1021/acsami.5b00643
ACS Appl. Mater. Interfaces 2015, 7, 5624−5628

950 nm) as revealed by *in situ* ion sputtering within the XPS instrument and measurements made on the bottom of the films (Figure S2, Supporting Information).

The morphologies of pure Cu_2O and Zn:Cu_2O films are shown in Figure 2a (a larger version is also provided in Figure S3, Supporting Information). All films exhibited clearly faceted, micron-scale grains that are typical of Cu_2O thin films grown under low pH conditions at sufficiently large cathodic potentials to induce a high density of nucleation sites.[22] At low doping concentrations, the incorporation of zinc does not lead to any large change in morphology, although there is an obvious second phase visible in the film containing the largest amount of zinc ([Zn]/[Cu] = 0.236, deposited using 0.016 M $NaClO_4$ at −0.08 V vs Ag/AgCl). At such a large [Zn]/[Cu] value, the amount of zinc present in this sample likely exceeds the saturation point of zinc doping into the Cu_2O lattice. Interestingly, the second phase does not show up in the XRD pattern for this film (Figure 2b), which may be because the total amount of this second phase is too small to be detected by XRD and/or is amorphous.

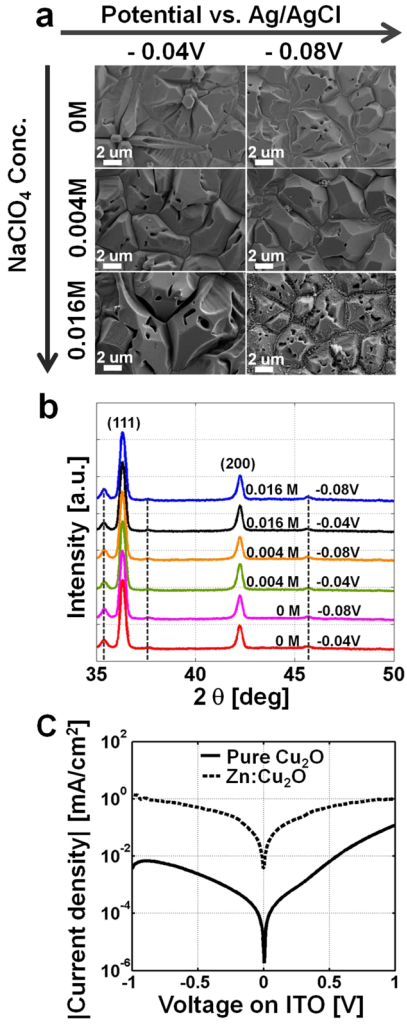

Figure 2. (a) Top view SEM images of films electrodeposited using $NaClO_4$ concentrations of: 0, 0.004, and 0.016 M NaClO4 at applied potentials of −0.04 or −0.08 V vs Ag/AgCl. (b) XRD patterns corresponding to the six films shown in panel (a). The dashed vertical lines indicate diffraction peaks due to the ITO substrate. (c) Current−voltage characteristics of films electrodeposited at −0.06 V vs Ag/AgCl with 0 M $NaClO_4$ (yielding pure Cu_2O) or 0.004 M $NaClO_4$ (Zn:Cu_2O).

The XRD patterns shown in Figure 2b reveal that all of the films, including both the Zn:Cu_2O films as well as the pure Cu_2O films, display only peaks assigned to cubic Cu_2O (cuprite, JCPDS No. 78−2076). It should be noted that no peaks that could be assigned to pure ZnO are present in the diffraction spectra of the Zn:Cu_2O films, which further suggests that zinc cations are incorporated into the Cu_2O lattice. Additional evidence for the formation of zinc-doped Cu_2O rather than a mixture of amorphous ZnO and polycrystalline Cu_2O can be seen in the optical absorption data of Zn:Cu_2O versus pure Cu_2O films (Figure S4, Supporting Information), wherein the incorporation of Zn results in a shift in the optical band gap to larger energies.[30] The presence of zinc in the Zn:Cu_2O films does not change the relative orientation or peak widths compared to the pure Cu_2O film XRD pattern, indicating that Zn doping causes little change to the Cu_2O lattice and no structural distortion, which was also observed by Heng and co-workers in Zn-doped Cu_2O microcrystals grown by a hydrothermal route.[30] This may be because Cu^+ and Zn^{2+} have similar ionic radii values of 0.46 and 0.40 Å, respectively.[31]

Current−voltage characterization was first performed on Zn:Cu_2O and pure Cu_2O films electrodeposited at pH 5.8 on ITO electrodes using a liquid eutectic gallium−indium (EGaIn) soft top contact.[23] Figure 2c compares typical current−voltage curves measured for a pure Cu_2O film and for a Zn:Cu_2O film. SEM cross-sectional images revealed that both of these films had a thickness of ∼950 nm and exhibited similar roughness values (Figures S5 and S6, Supporting Information). The pure Cu_2O film exhibits a Schottky junction with the liquid metal, which is expected due to the mismatch between the Fermi level of the pure Cu_2O film and the work function of EGaIn.[22] In contrast, the contact behavior between the Zn:Cu_2O film and EGaIn is seen to be Ohmic instead of rectifying. In addition, the conductivity of the Zn:Cu_2O film is larger than that of the pure Cu_2O film, as indicated by the greater current density under forward bias (positive potential on ITO). These observations may be attributed to the zinc dopant, which raises the Fermi level closer to the work function of the liquid metal located at ∼4.2 eV below vacuum, indicating the reduced p-type character of the film.

Electrodeposited Cu_2O homojunction photovoltaic devices were fabricated with the structures glass/ITO/p-Cu_2O (750 nm)/Zn:Cu_2O (250 nm)/Al/Au and glass/ITO/p-Cu_2O (750 nm)/pure Cu_2O (250 nm)/Al/Au. The [Zn]/[Cu] in the Zn:Cu_2O top layer devices was 0.042. Both types of PV structures contained identically prepared 750 nm thick p-Cu_2O films electrodeposited at high pH onto ITO-coated glass substrates (see Figure S7, Supporting Information); SEM images of the top view and cross-section of the p-Cu_2O film on ITO are shown in Figure 3a. When electrodeposited onto this p-Cu_2O layer, the top surfaces of the 250 nm-thick Zn:Cu_2O and pure Cu_2O films (both grown at pH 5.8) exhibited similar morphologies (Figure 3b and c), which confirms that the presence of the zinc dopant does not substantially change the Cu_2O film morphology. However, comparison of Figure 3b and Figure 2a reveals a clear difference in the appearance of the Zn:Cu_2O films grown on p-Cu_2O and ITO; the p-Cu_2O layer appears to template the growth of the Zn-doped layer. This templating effect can be confirmed by examining the XRD patterns of the bottom p-Cu_2O layer and the p-Cu_2O/Zn:Cu_2O homojunction, both of which exhibit greater relative ⟨111⟩

DOI: 10.1021/acsami.5b00643
ACS Appl. Mater. Interfaces 2015, 7, 5624−5628

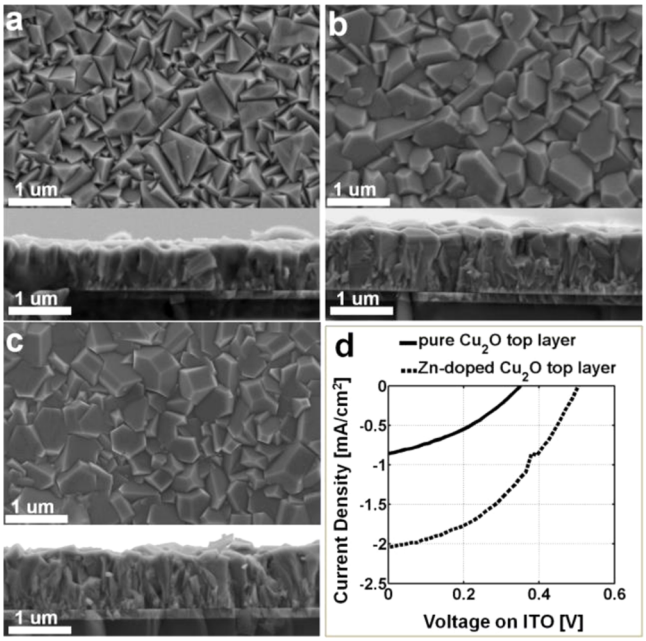

Figure 3. (a–c) SEM top view (top) and cross-sectional view (bottom) images of electrodeposited films grown on ITO-coated glass substrates: (a) 750 nm thick p-Cu_2O film, (b) homojunction with an ~250 nm Zn:Cu_2O layer ([Zn]/[Cu] = 0.042) electrodeposited on top of the p-Cu_2O film, and (c) homojunction with an ~250 nm pure Cu_2O layer electrodeposited on top of the p-Cu_2O film. (d) Current density–voltage characteristics of the two homojunction PV devices under 100 mW/cm^2 simulated solar illumination.

orientation compared to the Zn:Cu_2O film grown on ITO (Figure S8, Supporting Information).

The PV performances of both devices were measured under 100 mW/cm^2 simulated solar illumination with typical current density–voltage characteristics shown in Figure 3d. Devices containing the Zn:Cu_2O top layer exhibited substantially improved performance (average PCE of 0.42 ± 0.02%, V_{OC} of 0.50 ± 0.01 V, J_{SC} of 2.02 ± 0.06 mA/cm^2, and a fill factor of 42 ± 0.2%) compared to devices containing a pure Cu_2O top layer (PCE of 0.14 ± 0.05%, V_{OC} of 0.33 ± 0.02 V, J_{SC} of 1.08 ± 0.27 mA/cm^2, and a fill factor of 38 ± 3%). The Zn-doped devices showed an open circuit voltage of 0.5 V, indicating that the minimum difference between the quasi-Fermi level energies of the p-Cu_2O and the Zn:Cu_2O films is 0.5 V. This increased quasi-Fermi level energy difference is due to the zinc dopant. Furthermore, the greater than 2-fold increase in short circuit current density can be attributed to the higher conductivity of the Zn:Cu_2O film. Although the highest PCE obtained here (0.44%) is somewhat lower than the best electrodeposited Cu_2O homojunction PV reported to date (~1%),[9] our average cell efficiency effectively tripled through the use of the Zn:Cu_2O top layer. Further optimization of the Cu_2O layer thicknesses and [Zn]/[Cu] is expected to produce even higher gains in the near future.

In conclusion, zinc has been successfully incorporated into Cu_2O films using a single step electrodeposition. [Zn]/[Cu] increased exponentially with larger cathodic potential and approximately doubled when the initial sodium perchlorate concentration was increased from 0.004 to 0.016 M. The presence of the zinc dopant did not induce Cu_2O lattice distortion or any large change in film morphology. Zinc dopants increased the Fermi level and enabled facile charge carrier injection/extraction using the low work function metals EGaIn and Al. Higher Fermi level positioning and improved conductivity in the Zn:Cu_2O films enabled substantially improved performance in an electrodeposited Cu_2O homojunction PV device. The general strategy described here may also be more broadly applicable to help realize the successful co-deposition of Cu_2O with other metal cations via electrodeposition for a broad array of applications.

■ ASSOCIATED CONTENT

Supporting Information

Experimental details, additional XPS spectra, additional SEM images, thin film optical absorption data, AFM images, a schematic diagram of a Cu_2O homojunction PV device, and additional XRD patterns. This material is available free of charge via the Internet at http://pubs.acs.org.

■ AUTHOR INFORMATION

Corresponding Author

*E-mail: matthew.panzer@tufts.edu.

Author Contributions

C.Z. and M.P. contributed equally to this study.

Notes

The authors declare no competing financial interest.

■ ACKNOWLEDGMENTS

This work utilized the Center for Nanoscale Systems (CNS) at Harvard University, supported by NSF Award ECS-0335765, and the MRSEC Shared Experimental Facilities at MIT, supported by NSF Award DMR-08-19762.

■ REFERENCES

(1) Yang, H.; Ouyang, J.; Tang, A.; Xiao, Y.; Li, X.; Dong, X.; Yu, Y. Electrochemical Synthesis and Photocatalytic Property of Cuprous Oxide Nanoparticles. *Mater. Res. Bull.* **2006**, *41*, 1310–1318.

(2) Dong, C.; Zhong, M.; Huang, T.; Ma, M.; Wortmann, D.; Brajdic, M.; Kelbassa, I. Photodegradation of Methyl Orange Under Visible Light by Micro-Nano Hierarchical Cu_2O Structure Fabricated by Hybrid Laser Processing and Chemical Dealloying. *ACS Appl. Mater. Interfaces* **2011**, *3*, 4332–4338.

(3) Coey, J. M.; Venkatesan, M.; Fitzgerald, C. B. Donor Impurity Band Exchange in Dilute Ferromagnetic Oxides. *Nat. Mater.* **2005**, *4*, 173–9.

(4) Du, Y.; Zhang, N.; Wang, C. Photo-Catalytic Degradation of Trifluralin by SnO_2-doped Cu_2O Crystals. *Catal. Commun.* **2010**, *11*, 670–674.

(5) Zhang, L.; Jing, D.; Guo, L.; Yao, X. In Situ Photochemical Synthesis of Zn-Doped Cu_2O Hollow Microcubes for High Efficient Photocatalytic H_2 Production. *ACS Sustainable Chem. Eng.* **2014**, *2*, 1446–1452.

(6) McShane, C. M.; Siripala, W. P.; Choi, K. S. Effect of Junction Morphology on the Performance of Polycrystalline Cu_2O Homojunction Solar Cells. *J. Phys. Chem. Lett.* **2010**, *1*, 2666–2670.

(7) Han, K.; Tao, M. Electrochemically Deposited p–n Homojunction Cuprous Oxide Solar Cells. *Sol. Energy Mater. Sol. Cells* **2009**, *93*, 153–157.

(8) Jiang, T.; Xie, T.; Yang, W.; Chen, L.; Fan, H.; Wang, D. Photoelectrochemical and Photovoltaic Properties of p–n Cu_2O Homojunction Films and Their Photocatalytic Performance. *J. Phys. Chem. C* **2013**, *117*, 4619–4624.

(9) McShane, C. M.; Choi, K. S. Junction Studies on Electrochemically Fabricated p–n Cu_2O Homojunction Solar Cells for Efficiency Enhancement. *Phys. Chem. Chem. Phys.* **2012**, *14*, 6112–6118.

(10) Wei, H. M.; Gong, H. B.; Chen, L.; Zi, M.; Cao, B. Q. Photovoltaic Efficiency Enhancement of Cu_2O Solar Cells Achieved by

DOI: 10.1021/acsami.5b00643
ACS Appl. Mater. Interfaces 2015, 7, 5624–5628

Controlling Homojunction Orientation and Surface Microstructure. *J. Phys. Chem. C* **2012**, *116*, 10510−10515.
(11) Ishizuka, S.; Kato, S.; Okamoto, Y.; Akimoto, K. Hydrogen Treatment for Polycrystalline Nitrogen-Doped Cu_2O Thin Film. *J. Cryst. Growth* **2002**, *237*−*239*, 616−620.
(12) Kale, S. N.; Ogale, S. B.; Shinde, S. R.; Sahasrabuddhe, M.; Kulkarni, V. N.; Greene, R. L.; Venkatesan, T. Magnetism in Cobalt-Doped Cu_2O Thin Films without and with Al, V, or Zn Codopants. *Appl. Phys. Lett.* **2003**, *82*, 2100−2103.
(13) Sieberer, M.; Redinger, J.; Mohn, P. Electronic and Magnetic Structure of Cuprous Oxide Cu_2O Doped with Mn, Fe, Co, and Ni: A Density Functional Theory Study. *Phys. Rev. B* **2007**, *75*, 035203.
(14) Martínez-Ruiz, A.; Moreno, M. G.; Takeuchi, N. First Principles Calculations of the Electronic Properties of Bulk Cu_2O, Clean and Doped with Ag, Ni, and Zn. *Solid State Sci.* **2003**, *5*, 291−295.
(15) Isseroff, L. Y.; Carter, E. A. Electronic Structure of Pure and Doped Cuprous Oxide with Copper Vacancies: Suppression of Trap States. *Chem. Mater.* **2013**, *25*, 253−265.
(16) Brandt, I. S.; Lima, E., Jr.; Tumelero, M. A.; Acuna, J. J. S.; Viegas, A. D. C.; Zysler, R. D.; Pasa, A. A. Magnetic Characterization of Co-Doped Cu_2O Layers. *IEEE Trans. Magn.* **2011**, *47*, 2640−2642.
(17) Kemell, M.; Dartigues, F.; Ritala, M.; Leskela, M. Electrochemical Preparation of In and Al Doped ZnO Thin Films for $CuInSe_2$ Solar Cells. *Thin Solid Films* **2003**, *434*, 20−23.
(18) Ramirez, D.; Alvarez, K.; Riveros, G.; Tejos, M.; Lobos, M. G. New Insights on the Doping of ZnO Films with Elements from Group IIIA Through Electrochemical Deposition. *J. Solid State Electrochem.* **2014**, *18*, 2829−2884.
(19) Han, X.; Han, K.; Tao, M. Characterization of Cl-Doped n-type Cu_2O Prepared by Electrodeposition. *Thin Solid Films* **2010**, *518*, 5363−5367.
(20) Wu, S.; Yin, Z.; He, Q.; Lu, G.; Zhou, X.; Zhang, H. Electrochemical Deposition of Cl-Doped n-type Cu_2O on Reduced Graphene Oxide Electrodes. *Chem. Mater.* **2011**, *21*, 3467−3470.
(21) Pauporte, T.; Goux, A.; Kahn-Harari, A.; Tacconi, N. D.; Chenthamarakshan, C. R.; Rajeshwar, K.; Lincot, D. Cathodic Electrodeposition of Mixed Oxide Thin Films. *J. Phys. Chem. Solids* **2003**, *64*, 1737−1742.
(22) Osherov, A.; Zhu, C.; Panzer, M. J. Role of Solution Chemistry in Determining the Morphology and Photoconductivity of Electrodeposited Cuprous Oxide Films. *Chem. Mater.* **2013**, *25*, 692−698.
(23) Zhu, C.; Osherov, A.; Panzer, M. J. Suface Chemistry of Electrodeposited Cu_2O Films Studied by XPS. *Electrochim. Acta* **2013**, *111*, 771−778.
(24) Illy, B. N.; Cruickshank, A. C.; Schumann, S.; Campo, R. D.; Jones, T. S.; Heutz, S.; McLachlan, M. A.; McComb, D. W.; Riley, D. J.; Ryan, M. P. Electrodeposition of ZnO Layers for Photovoltaic Applications: Controlling Film Thickness and Orientation. *J. Mater. Chem.* **2011**, *21*, 12949−12957.
(25) Qiu, J.; Guo, M.; Wang, X. Electrodeposition of Hierarchical ZnO Nanorod−Nanosheet Structures and Their Applications in Dye-Sensitized Solar Cells. *ACS Appl. Mater. Interfaces* **2011**, *3*, 2358−2367.
(26) Islam, M. N.; Ghosh, T. B.; Chopra, K. L.; Acharya, H. N. XPS and X-ray Diffraction Studies of Aluminum-Doped Zinc Oxide Transparent Conducting films. *Thin Solid Films* **1996**, *280*, 20−25.
(27) Chen, M.; Pei, Z. L.; Sun, C.; Wen, L. S.; Wang, X. Surface Characterization of Transparent Conductive Oxide Al-Doped ZnO Films. *J. Cryst. Growth* **2000**, *220*, 254−262.
(28) Mar, L. G.; Timbrell, P. Y.; Lamb, R. N. An XPS Study of Zinc Oxide Thin Film Growth on Copper Using Zinc Acetate as a Precursor. *Thin Solid Films* **1993**, *223*, 341−347.
(29) Lin, B.; Chen, S.; Shen, P. (Zn,H)-Codoped Copper Oxide Nanoparticles via Pulsed Laser Ablation on Cu−Zn Alloy in Water. *Nanoscale Res. Lett.* **2012**, *7*, 272−297.
(30) Heng, B.; Xiao, T.; Tao, W.; Hu, X.; Chen, X.; Wang, B.; Sun, D.; Tang, Y. Zn Doping-Induced Shaped Evolution of Microcrystals: The Case of Cuprous Oxide. *Cryst. Growth Des.* **2012**, *12*, 3998−4005.
(31) Nolan, M.; Elliott, S. D. Tuning the Transparency of Cu_2O with Substitutional Cation Doping. *Chem. Mater.* **2008**, *20*, 5522−5531.

DOI: 10.1021/acsami.5b00643
ACS Appl. Mater. Interfaces 2015, 7, 5624−5628